ORNL/CP-97879

CONF-980545--

Instrumentation and Controls Division

^{252}CF-SOURCE-CORRELATED TRANSMISSION MEASUREMENTS FOR URANYL FLUORIDE DEPOSIT IN A 24-IN.-OD PROCESS PIPE*

T. Uckan, M. S. Wyatt+, J. T. Mihalczo,
T. E. Valentine, J. A. Mullens, and T. F. Hannon++

Oak Ridge National Laboratory, Oak Ridge, TN 37830, USA
+Depart. of Nuclear Eng., The University of Tennessee, Knoxville, TN 37996, USA
++Central Engineering Services, P.O. Box 2003, Oak Ridge, TN 37831, USA

Paper submitted to the
1998 Symposium on Radiation Measurements and Applications
The University of Michigan
Ann Arbor, Michigan
May 11-14, 1998

*Research sponsored by the U.S. Department of Energy, under contract DE-AC05-96OR22464 with Lockheed Martin Energy Research Corp., and DE-AC05-84OR21400 with Lockheed Martin Energy Systems, Inc.

DISCLAIMER

^{252}Cf-source-correlated transmission measurements for uranyl fluoride deposit in a 24-in.-OD process pipe*

T. Uckan, M. S. Wyatt+, J. T. Mihalczo, T. E. Valentine, J. A. Mullens, and T. F. Hannon++

Instrumentation and Controls Division

Oak Ridge National Laboratory, Oak Ridge, TN 37830, USA

+Department of Nuclear Engineering, The University of Tennessee, Knoxville, TN 37996, USA

++Central Engineering Services, P.O. Box 2003, Oak Ridge, TN 37831, USA

Abstract

Characterization of a hydrated uranyl fluoride ($UO_2F_2 \cdot nH_2O$) deposit in a 17-ft-long, 24-in.-OD process pipe at the former Oak Ridge Gaseous Diffusion Plant was successfully performed by using ^{252}Cf-source-correlated time-of-flight (TOF) transmission measurements. These measurements of neutrons and gamma rays through the pipe from an external ^{252}Cf fission source were used to measure the deposit profile and its distribution along the pipe, the hydration (or H/U), and the total uranium mass. The measurements were performed with a source in an ionization chamber on one side of the pipe and detectors on the other. Scanning the pipe vertically and horizontally produced a spatial and time-dependent radiograph of the deposit in which transmitted gamma rays and neutrons were separated in time. The cross-correlation function between the source and the detector was measured with the Nuclear Weapons Identification System. After correcting for pipe effects, the deposit thickness was determined from the transmitted neutrons and H/U from the gamma rays. Results were consistent with a later intrusive observation of the shape and the color of the deposit; i.e., the deposit was annular and was on the top of the pipe at some locations, demonstrating the usefulness of this method for deposit characterization.

*Research sponsored by the U.S. Department of Energy, under contract DE-AC05-96OR22464 with Lockheed Martin Energy Research Corp., and DE-AC05-84OR21400 with Lockheed Martin Energy Systems, Inc.

1. Introduction

The U. S. Department of Energy initiated the Deposit Removal Project in the East Tennessee Technology Park for safe removal of hydrated uranyl fluoride (UO_2F_2) deposits from process pipes and equipment in the K-29 building at the former Oak Ridge Gaseous Diffusion Plant (ORGDP). The deposits developed from moist air leakage into UF_6 gas lines; eventually, the UO_2F_2 became hydrated to form a UO_2F_2-H_2O mixture. Because hydrogen moderates neutrons, the hydrogen content [the ratio of H to U (H/U)] was one of the key parameters that determine the nuclear criticality safety of the deposit. Earlier nondestructive assay measurements by gamma ray spectroscopy identified one of the largest deposits [1], the Unit 2, Cell 7, B-Line Outlet process pipe (Fig. 1), called the "Hockey Stick," a 17-ft-long 24-in.-OD pipe that was estimated to contain a uniformly distributed uranium mass of 1,200 kg at 3.3% enrichment. A main concern was that if H/U were high enough (i.e., if H/U = 4), the ^{235}U could become critical [2] if the deposit distribution reconfigured to a favorable geometry. The previous measurements used passive neutron and gamma ray interrogation techniques for determining the deposit profile and its distribution. This gamma ray passive technique is susceptible to background radiation and self-shielding of gamma rays by the deposit; the correct deposit thickness or distribution could not be determined but only that it was uniformly distributed. To alleviate criticality safety concerns, data were required on the spatial distribution, hydrogen content, and total uranium mass of the deposit in order to safely remove materials. The objectives of the measurements were to image the deposit profile, to determine the H/U and total uranium mass of the deposit. This paper describes how the deposit was characterized by an active neutron and gamma-ray interrogation method using the californium-252 (^{252}Cf)-source-correlated time-of-flight (TOF) transmission [3] measurements.

2. Measurement method and analysis

For this active measurement method an external fission source was placed outside the pipe, and the time distribution of the transmitted neutrons and gamma rays after ^{252}Cf fission was measured. The interaction probabilities of neutrons and gamma rays with the deposit are distinct from each other. The neutron interaction probability for the high-energy neutrons is not very sensitive to H/U whereas gamma interaction strongly depends on density or H/U. The ability to separate the transmission of neutrons and gamma rays through the deposit by TOF timing provides a neutron and gamma ray radiograph of the deposit for measuring deposit thickness and the density (or H/U). The ^{252}Cf isotope is a convenient interrogation source because its spontaneous fission emits 2.32×10^6 neutrons/s/μg and 4.78×10^6 gamma rays/s/μg [4]. The neutrons and the gamma rays transmitted through the pipe were measured with plastic scintillators.

Neutron energy distribution was obtained by measuring time correlation of the neutrons through the pipe. This was accomplished by using the ^{252}Cf source in a parallel-plate ionization

chamber for obtaining a timing signal at the source from prompt neutrons and gamma rays resulting from the fission of ^{252}Cf. Because the time of fission was known, the TOF of transmitted neutrons or gammas arriving at the detector located opposite side of the pipe was measured. This time-correlated signature is equivalent to the right half of the cross-correlation function between the source ionization chamber (detector #1) and the detector (detector #2) (CCF12) and was equivalent to randomly pulsed neutron measurements [3]. The Nuclear Weapons Identification System (NWIS) processor, developed at the Oak Ridge Y-12 Plant [5, 6] for identification of nuclear weapons components in storage containers, provided the CCF12 [7] for these measurements.

2.1. Measurements of deposit profile

The measurements were performed by placing the source on one side of the pipe and a pair of detectors on the other side (Fig. 2). The measured intensity of neutrons, $I(E)$ of energy E, transmitted through the pipe is approximated by

$$I(E) = I_{air}(E)\exp[-\Sigma_t(E)d - 2\Sigma_p w] = I_o\exp[-\Sigma_t(E)d] , \quad (1)$$

where $I_{air}(E)$ is the intensity of neutrons measured in air; $\Sigma_t(E)$ and Σ_p are the total macroscopic neutron cross sections of the deposit and the pipe, respectively; d is the total deposit thickness along the measurement path; $w = 0.375$ in., the wall thickness of the pipe (carbon steel). Here $I_o = I_{air}(E)\exp[- 2\Sigma_p w]$ is the intensity of neutrons transmitted through the empty pipe. Both $I(E)$ and $I_o(E)$ are measured. The value of $\Sigma_t(E)$ for a hydrated UO_2F_2 deposit is known as a function of E and H/U [8]. At low neutron energies (below 1.5 MeV) Σ_t is sensitive to both changes in H/U and variations in E. At high energies (above 6 MeV), Σ_t is constant with H/U and is not a strong function of E [8]. In order for Eq. (1) to be valid the neutron scattering from the surrounding deposit into the detectors needs to be minimized. This was accomplished by measuring relatively higher-energy neutrons ($E \sim 8$ MeV) because scattering would reduce the neutron energy below 8 MeV so that neutrons that scattered into the detector would be counted later than the time corresponding to 8 MeV. Monte Carlo code calculations (MCNP-DSP) [9] were used to verify the assumption that measurements of the deposit thickness from high-energy neutrons are not sensitive to geometry or inscattering effects. With a neutron energy of 8.5 MeV selected, the approximations of Eq. (1) are valid and the total deposit thickness can be obtained

$$d = - \ln(I/I_o) / \Sigma_t . \quad (2)$$

The variation of Σ_t is less than ±14% for a broad range of H/U values (0.6–16). To determine the deposit thickness from Eq. (2), the effects of the pipe were eliminated using empty pipe measurements for I_o. The CCF12 was obtained from the NWIS measurements for I(E) through the pipe with the deposit. Thus I/I_o at 8.5 MeV was obtained because the time of arrival and distance

between the source and the detector were known. The deposit thickness was determined from Eq. (2) and I/I_0. The pipe deposit image was obtained from vertical (y-axis) and horizontal (x-axis) scans (Fig. 2), in which the source and the detectors were moved simultaneously. From these measurements the total deposit thickness in the horizontal direction, $d_x(y)$, and in the vertical direction, $d_y(x)$, were obtained. The composite deposit image in the pipe was constructed from $d_x(y)$ and $d_y(x)$, and the result is further verified by source and the detector rotation measurements around the pipe.

2.2. Measurements of H/U

The density of the hydrated deposit is directly related to H/U in the deposit and can be represented as $UO_2F_2 \cdot nH_2O$, where H/U = $2n$. The attenuation of gamma rays depends on the deposit thickness and density (or H/U). The mass attenuation coefficient μ_i/ρ_i and the density ρ_i for the elements of the deposit are known. The intensity of the gamma rays transmitted through the deposit is expressed as $I^\gamma(E) = C^\gamma N^\gamma(E)\exp[-2\mu_w w - \sum_i(\mu_i/\rho_i)\rho_i d]$, where N^γ is normalized to unity so that C^γ is the number of prompt gamma rays per fission, μ_w is the linear attenuation coefficient of the pipe. Ideally, the CCF12 of the gamma rays is an impulse function, but due to the finite time resolution of NWIS, CCF12 has a finite broadening. Thus the total counts for the transmitted gamma rays Γ are the total counts integrated under the gamma peak in CCF12, which is $\Gamma = \int_0^\infty dE\, I^\gamma(E) = C^\gamma \int_0^\infty dE\, N^\gamma \exp[-2\mu_w w - \sum_i(\mu_i/\rho_i)\rho_i d]$. Normalizing Γ to the empty pipe measurements of Γ_o leads to

$$\Gamma/\Gamma_o = \int_0^\infty dE\, N^\gamma \exp[-2\mu_w w - \sum_i(\mu_i/\rho_i)\rho_i d] \,/ \int_0^\infty dE\, N^\gamma \exp[-2\mu_w w] = F(\text{H/U}, d)\,. \qquad (3)$$

When N^γ, μ_w for the pipe and μ_i/ρ_i [8] for the elements of the deposit are known, F(H/U, d) is calculated for H/U values and deposit thicknesses. As expected, F(H/U, d) increases with H/U while decreases with d.

H/U is then determined as follows. First, the deposit thickness is obtained from the 8.5-MeV neutrons transmitted across the deposit pipe. The measured Γ/Γ_o is then used for H/U determination in F(H/U, d). For thin deposits of ≤ 2 cm and $\Gamma/\Gamma_o \le 1$, the determination of H/U is very sensitive; i.e., an error of 0.5 cm can correspond to a large variation in H/U for $\Gamma/\Gamma_o \sim 1$. The results can be improved through iterative technique using the initial d and H/U values: (1) From the neutron transmission measurements at 8.5 MeV, a first estimate of d is obtained by using a Σ_t averaged over H/U because Σ_t only varies ±15% for H/U = 0.6–16. (2) By utilizing this initial d together with the gamma ray transmission measurements in F(H/U, d), the corresponding new H/U is obtained. (3) The value of Σ_t can now be refined because a better estimate of H/U is known, and in turn, a refined d can be recalculated [Eq. (2)]. (4) With the refined d, the H/U value can be further improved using the gamma transmission data in F(H/U, d).

This iterative process can continue until the improvements on the values of d and H/U are small.

3. Measurement hardware and description of measurements

The NWIS measurement hardware [10] is composed of a ^{252}Cf source contained in an ionization chamber, a pair of detectors for measuring neutrons and gamma rays, detector electronics, data-processing boards, and a computer for data acquisition and display. Electronic pulses from the source and detectors are sampled in time with 1 GHz of data sampling of the input pulses from the detectors, producing time-dependent source and detector responses. The system time resolution is ≤ 2 ns. The source is 1-in.-OD and 1.25-in. long, with about 0.6 μg of ^{252}Cf electroplated onto one plate. A timed electrical pulse occurs each time the source emits neutrons and gamma rays. An high-gain fast amplifier increases the pulse amplitude, which is input to a constant-fraction discriminator that eliminates unwanted pulses with appropriate thresholds and produces an output timing pulse that is independent of the incoming signal height and has constant amplitude and adjustable width. The output of the discriminator is input to a delay module that delays the arrival time of pulses from the source to the data processor. The detectors consist of plastic scintillators mounted on photomultiplier tubes. The 3.75 × 3.75 in. scintillators are enclosed in aluminum cans 0.125 in. thick and 4 × 4 in. square, with a 0.25-in.-thick lead shield on the sides (Fig. 2). The detector anode signal is input to a discriminator whose output is input to the data processor. The data acquisition components of the processor are two electronic boards. The data capture and compression modules acquire the signals as input to a data processor that inputs the data to the computer for additional processing and storage.

The measurements were performed on the pipe at $L = 40$, 54, 80, 104, 133, and 163 in. as indicated in Fig. 1. These locations along the midplane of the pipe were measured from the flange ($L = 0$ in.) located by the left side of the valve (Fig. 1). The source and the detectors were placed on a fixture (Fig. 2) that allowed both the source and the detectors to scan vertically and horizontally and to be rotated. The two detectors were placed side-by-side along the pipe's z-axis (Figs. 1 and 2) such that the distance between the centers of the detectors was 4.5 in. The pipe was scanned vertically and horizontally every 2 in. and the source and the detectors were rotated 360^0 in 30^0 intervals whenever clearance permitted. Before, during, and after the measurements, neutron detector efficiency measurements in air were performed with the source and the detectors spaced 40 in. apart. Peak neutron efficiency was about 50% and for 8.5-MeV neutrons was about 35–38%. This efficiency was maintained within 5% during the measurements. The discriminator threshold was set at 0.2 MeV for gamma rays and 1 MeV for neutrons. The measurement time was ~12 min of NWIS processing. The measurement reproducibility was checked by repeated measurements at each measurement location on the pipe at different times. The results varied by less than 10%. Calibration measurements were also performed on an identical empty pipe.

4. Measurement results

4.1. Deposit profile and its distribution along the Hockey Stick

A typical time signature is shown in Fig. 3. The CCF12 counts are normalized to the number of ^{252}Cf fissions. The first peak represents the TOF ($\tau \sim 2$ ns) of prompt gamma rays from ^{252}Cf fission while the second peak ($\tau \sim 29$ ns) is mainly from transmitted fission neutrons having an average energy of $E = 2.13$ MeV [4]. The time spread of the gamma peak is due to the finite time resolution of the measuring system. Counts for $\tau > 80$ ns represent the uncorrelated background. From these data, corrected for the background, the intensity of the transmitted neutrons at $E = 8.5$ MeV is obtained at their TOF of $\tau = 15$ ns. The measurement results from the detector #2 for the deposit profiles along the pipe are presented for $L = 40$, 54, 80, 104, 133, and 163 in. (a) $L = 40$ in.: This location was near the valve (Fig. 1), where the air leakage occurred. This was a transition section of the pipe connecting the 20-in.-OD pipe and the 24-in.-OD pipe (Fig. 1). Vertical and the horizontal scans were performed. The scans were limited to ±8 in. because at 10 in. part of the detector viewed the source directly. Measurements were also performed with a clean transition section to remove wall effects. The gamma portion of the CCF12 was used to calculate H/U. Because of the extreme sensitivity of this method to thin deposits, only data for deposits thicker than 1.25 in. were used to determine H/U. The iterative procedure was performed to refine of the deposit thickness and H/U. Data from the vertical and the horizontal scans were used to construct the profile [Fig. 4(a)]. The profile show that, contrary to expectation, the deposit existed on the top of the pipe and that the bottom contains very little deposit material. This result was confirmed later with the intrusive look and also when the pipe was cut (Fig. 5) The cut location was at L = 30 in. and did not corresponds to the measurement location. The deposit had an annular shape because increasing displacement from the midplane yielded an increasing deposit thickness. The deposit profile was symmetric from left to right. (b) $L = 54$ in.: Vertical and the horizontal scans were performed, as was a source-detector rotation. The source-detector scans were limited to ±10 in. to avoid viewing the source directly at 12 in. The average H/U obtained from the iterative procedure used for Σ_t to obtain the deposit thickness. The deposit thickness varied from $d\ (x = 0) = 1.83$ in. to $d\ (x = 2$ in.$) = 2.35$ in. Because the vertical scans revealed that very little deposit material existed in the bottom of the pipe, the data from the horizontal scan were used to calculate the deposit thickness at the top of the pipe. This result was confirmed by the intrusive look performed later, again not at the measurement location. Figure 4(b) presents the estimated deposit profile obtained by incorporating data from the vertical, horizontal, and the rotation scans. The profile was similar to that of $L = 40$ in.; most of the deposit was on the top of the pipe (Fig. 6). The results indicated the existence of strong deposit irregularities. The intrusive observations later showed that deposit was not smooth in this region up to the valve but consisted of large, closely grouped nodules

(Figs. 5 and 7). (c) L = 80 in.: This location was at the curved elbow section of the pipe directly below the expansion joint (Fig. 1). Only a single vertical scan was performed, due to the interference of the expansion joint, and the estimated profile is given in Fig. 4(c). Results indicate that the deposit existed again mainly on the upper part of the pipe. (d) L = 104 in.: This location was on the vertical riser, immediately above the expansion joint (Fig. 1). The vertical and the horizontal scans indicated that the deposit was more symmetric [Fig. 4(d)], with deposit material appearing in the bottom of the pipe, where none had been seen in previous locations. Data from the source-detector rotation measurements suggested a lack of material at one angular position on the pipe, as indicated by a sudden dips in the estimated deposit thickness at 60° and 240° and confirmed by the horizontal scan data. This result was confirmed later when the pipe was cut (Fig. 8). (e) L = 133 in.: Vertical and the horizontal scans were performed, and the profile is given in Fig. 4(e). The measured thicknesses had less irregularity from location to location at the top of the riser of the pipe. The profile became increasingly symmetric further up the vertical riser, although there was still a slight tendency for more deposit material to exist in the upper half of the pipe than in the lower region. (f) L = 163 in.: This location was the highest position on the vertical riser, about 10 ft from the floor. Measured vertical and horizontal source and detector data were used to estimate the deposit profile given in Fig. 4(f). The deposit was symmetric compared with those measured at to the rest of the locations and was thinner than the deposit in the previous location.

4.2. *Hockey Stick H/U ratio*

The deposit profile results were used with the gamma ray attenuation measurements to obtain the H/U values. To eliminate the effect of the extreme sensitivity of thin deposits on resolving the value of H/U, deposits less than 1 in. thick were not used in the analysis. About 32 measurements of H/U found from the iterative procedure satisfied the criterion. The measured H/U from the detector #2 (see Sect. 5 for the detector #3 results) had an average value of 3.4 ± 0.25 where the uncertainty is the standard deviation of the mean.

4.3. *Uncertainty for the deposit thickness measurements*

The measurement uncertainty for the deposit thickness $\Delta d/d$ can be estimated from Eq. (2) by making use of the method of error propagation: $\Delta d/d = \pm\{(\Delta\Sigma_t/\Sigma_t)^2 + [(\Delta I_o/I_o)^2 + (\Delta I/I)^2]/(d\Sigma_t)^2\}^{0.5}$. The upper bound of $\Delta d/d$ can be found by using a relatively thinner deposit thickness of d ~ 1 in. The value $\Delta d/d \leq \pm 17\%$ is obtained from $\Delta I_o/I_o = \Delta I/I \approx \pm 5\%$ as a typical value for the measurements, $\Delta\Sigma_t/\Sigma_t \approx \pm 3\%$ and Σ_t (H/U = 3.4) ≈ 0.165 cm^{-1} from the neutron cross-section data [8] for measured H/U = 3.4 ± 0.25.

4.4. *Hockey Stick total uranium mass*

The total uranium mass of the deposit was obtained by using the deposit profile results along

the pipe together with H/U, which is related to the uranium deposit density ρ_u [10]. A measurement segment of the pipe having a length of L_i, which is defined by the midpoints between measurement locations on either side of the measurement location L, was utilized for calculating the deposit volume. The deposit volume V_i of each measurement segment i was calculated from the deposit thickness and its shape, assuming that, within the measurement segment, the deposit profile remained uniform. An average deposit thickness $\bar{d}_i$ for the segment can be obtained by averaging the thicknesses given on the deposit profile; thus $\bar{d}_i = (1/N_i)\sum_j d_j$, with $j = 1, N_i$, where d_j is the deposit thickness given for each point on the profile, and N_i is the total number of points on the profile (indicated with arrows in Fig. 4). This approach is equivalent to making a surface area average of the deposit profile. The total deposit volume V_d can then be found from the volume of the each measurement segment V_i as $V_d = \sum_i V_i = \sum_i \pi L_i \bar{d}_i (D - \bar{d}_i)$, with $i = 1, N$, where L_i is the length of the measurement segment measured on the midplane of the pipe, N is the number of measurement locations, and D is the inner pipe diameter. The deposit volume of the each segment presented in Table 1 is based on the results of measured deposit profiles for $N = 6$ locations. The total deposit volume then becomes $V_d \approx 0.142$ m^3. The density of the uranium in the HS deposit is obtained from $\rho_u = [4.96 - 0.32 \times (H/U)]$ g/cc, valid for H/U ≤ 4 in the water-moderated mixtures of uranyl fluoride [11]. Using this for ρ_u and its associated uncertainty, $\Delta\rho_u = [0.32 \times \Delta(H/U)]$ g/cc, $\rho_u = (3.87 \pm 0.08)$ g/cc is found for the measured hydration level of H/U = 3.4 ± 0.25. The total uranium mass $M_u = \rho_u \times V_d$, and the uncertainty $\Delta M_u/M_u = \pm[(\Delta\rho_u/\rho_u)^2 + (\Delta d/d)^2]^{0.5}$, gives $M_u = 552 \pm 93$ kg for the data from detector #2.

5. Observations and discussion

The inside of pipe was surveyed intrusively to prepare a work plan before the deposit was removed. These measurement results were utilized for selecting the locations on the pipe for the visual observations. An articulated fiber-optic camera was inserted into the pipe at the top of the riser and from $L = 68$ in. on the side of the pipe about 5 in. below the midplane. A special tool for measuring the deposit thickness was also inserted from the bottom of the pipe at $L = 41$ in., located at the transition section, and at $L = 74$ in., located around the elbow region. In general, the intrusive observations were in good agreement with the deposit measurements. For example, most of the deposit was on the top of the pipe, from the valve to the elbow region; that is, $L = 40$ to 80 in. The deposit in this region was not smooth, but mostly consisted of large, closely grouped nodules (Figs. 6 and 7). The detector #3 data indicated the existence of large irregularities in the deposit thickness over a distance of 4.5 in. between the two detector locations. The intrusively measured deposit thicknesses at $L = 41$ in. and 74 in. were 1.5 and 0.875 in., respectively, and 0.125 in. on the bottom in both places. These intrusive measurements were also consistent with the profile measurements. The camera showed that the deposit profile became more smooth and

symmetrical up the riser section, correlating well with the measurements. The dominant orange and green-yellow colors (Figs. 6 and 7), which are related to the H/U of deposit [12], indicate H/U ~ 3 to 4 [12], which is consistent with the measurements. H/U = 3.4 ± 0.25. The pipe deposit has been successfully removed, and the estimated total uranium mass was 478.64 kg (with 50% uncertainty), which is consistent with the measured mass. The detector #3 results (H/U = 3.6 ± 0.24, M_u = 532 ± 90 kg) are also very consistent with the findings obtained from detector #2 data despite the large local differences between the two closely spaced (4.5 in.) detectors.

6. Conclusion

It was successfully demonstrated by the deposit characterization measurements that the active ^{252}Cf-source-correlated transmission measurement technique, which results in neutron and gamma ray radiographs, is a reliable method for nonintrusive hydrated uranyl fluoride deposit characterizations for obtaining the deposit distribution, the level of hydration, and the total uranium mass of the deposit. This technique can be applied to other UF_6 gaseous diffusion plants for deposit measurements or for other types of holdups in process pipes and other processes with nuclear material.

Acknowledgments

The authors thank C. P. Hall and P. Larson of the Deposit Removal Project and the valuable discussions with J. March-Leuba, J. K. Mattingly, and R. Perez are also greatly appreciated.

References

[1] T. F. Hannon et al., K-25 Site Doc. No. K/D-6048, January 1993.

[2] M. J. Haire and W. C. Jordan, Document No. K/ER-215, December 1995.

[3] J. T. Mihalczo, Nucl. Sci. Eng. **41**, 296 (1970).

[4] A. Prince, *Nuclear and Physical Properties of Cf-252*, p. 23 in Proc. of Symposium on Californium-252 CONF-681032 (ANS, New York, 1968).

[5] J. T. Mihalczo and V. K. Pare, "Nuclear Weapons Identification System (NWIS)," Arms Control and Nonproliferation Technologies, Third Quarter 1994, DOE/AN/ACNT-94C.

[6] J. E. Breeding et al., *New NWIS Processor for Fissile System Verification,* Institute of Nuclear Materials Management Meeting, Phoenix, Arizona, July 20-24, 1997.

[7] J. T. Mihalczo et al., *Physical and Mathematical Description of Nuclear Weapons Identification System (NWIS) Signatures*, Oak Ridge Y-12 Plant Rep. Y/LB-15, 946, 1997.

[8] The National Nuclear Data Center at Brookhaven National Laboratory, Upton, N.Y.

[9] T. E. Valentine and J. T. Mihalczo, Annals of Nuclear Energy **23**, 1271 (1996).

[10] J. T. Mihalczo et al., *NWIS Methodology*, Oak Ridge Y-12 Plant Rep. Y/LB-15, 953, 1997.

[11] W. C. Jordan, and J. C. Turner, ORNL/TM-12292, December 1992.

[12] M. G. Otey and R. A. LeDoux, J. Inorg. Nucl. Chem. **29**, 2249 (1967).

Figure captions

Figure 1. Unit 2, Cell 7, B-Line Outlet process pipe, called the "Hockey Stick."

Figure 2. ^{252}Cf source and the detectors placed on the pipe by means of a fixture for vertical, horizontal, and rotational measurements.

Figure 3. Time-correlated measurement signature shown for typical data, CCF12 cross-correlation function between ^{252}Cf source (detector #1) and detector #2.

Figure 4. Distribution of the deposit profile along the pipe.

Figure 5. Deposit and irregularities on the upper part of the pipe, confirmed as measured [Fig. 4(a)], looking toward the valve from the transition section, $L = 40$ in., when the pipe was cut.

Figure 6. Crescent shape of deposit, confirmed as measured [Fig. 4(b)], on the upper part of the pipe ($L = 36$–46 in.) obtained when the pipe was cut.

Figure 7. Intrusive look showing deposit nodule irregularities on the upper part of the pipe ($L =$ 40–80 in).

Figure 8. Deposit nodules and irregularities are shown on the upper part of the pipe together with the lack of material (shown with arrow) discussed in Fig. 4(d) for $L = 104$ in.

Table 1. Hockey Stick measurement segments for deposit volume calculations

Measurement location L (in.)	Segment location (in.)	Measurement segment length L_i (in.)	Average deposit thickness $\bar{d}_i$ (in.)	Segment volume V_i (in.^{3})[a]
40	0–47	47	0.38	1247
54	47–67	20	0.89	1250
80	67–92	25	0.87	1529
104	92–118.5	26.5	0.53	1002
133	118.5–148	29.5	0.97	2003
163	148–163	15	0.67	1675[b]

[a] Total deposit volume: $V_d = \sum_i V_i = 8706$ in.^{3} [b]Includes up to the top of the pipe, assuming that the deposit thickness varies linearly to 0.1-in. thickness at the top.

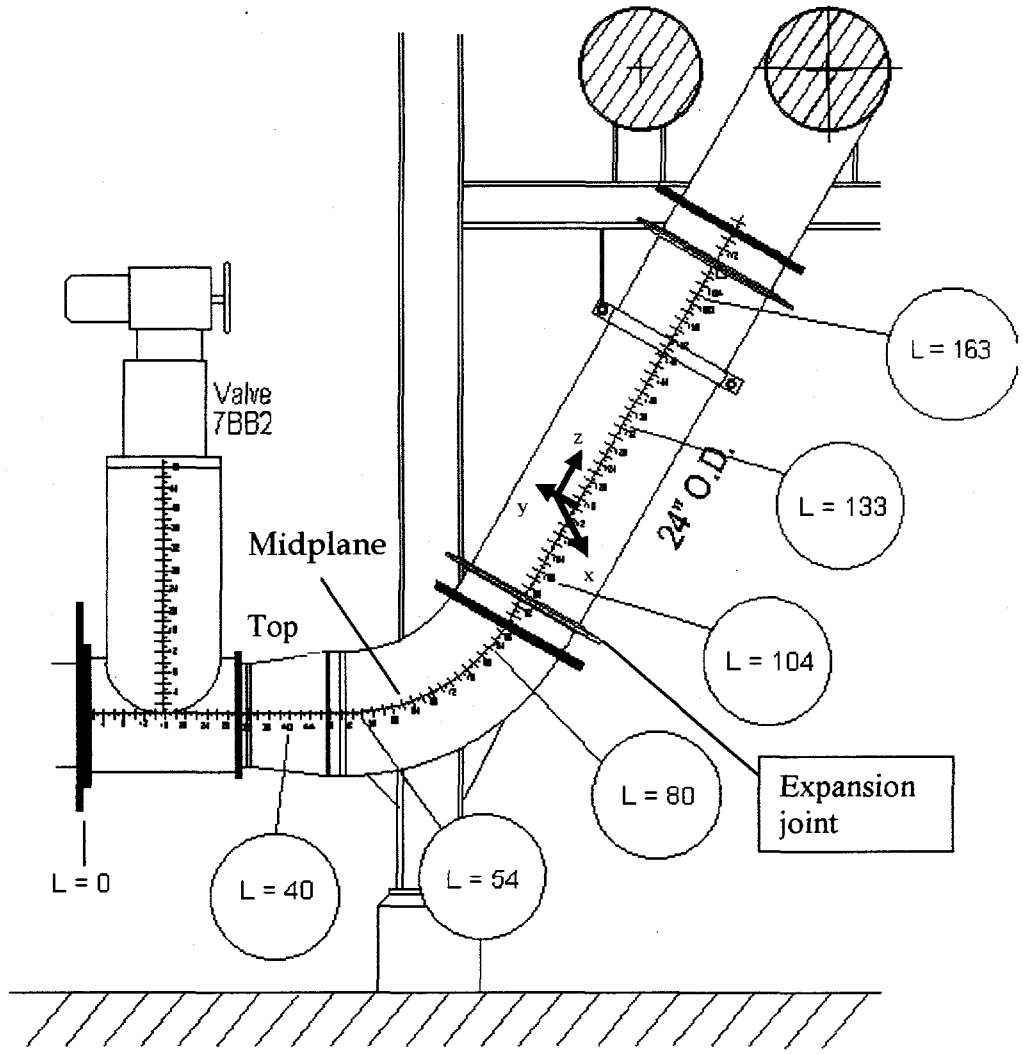
Valve
7BB2
Midplane
Top
L = 0
L = 40
L = 54
L = 80
L = 104
L = 133
L = 163
Expansion
joint
24" O.D.
z
y
x

Figure 1

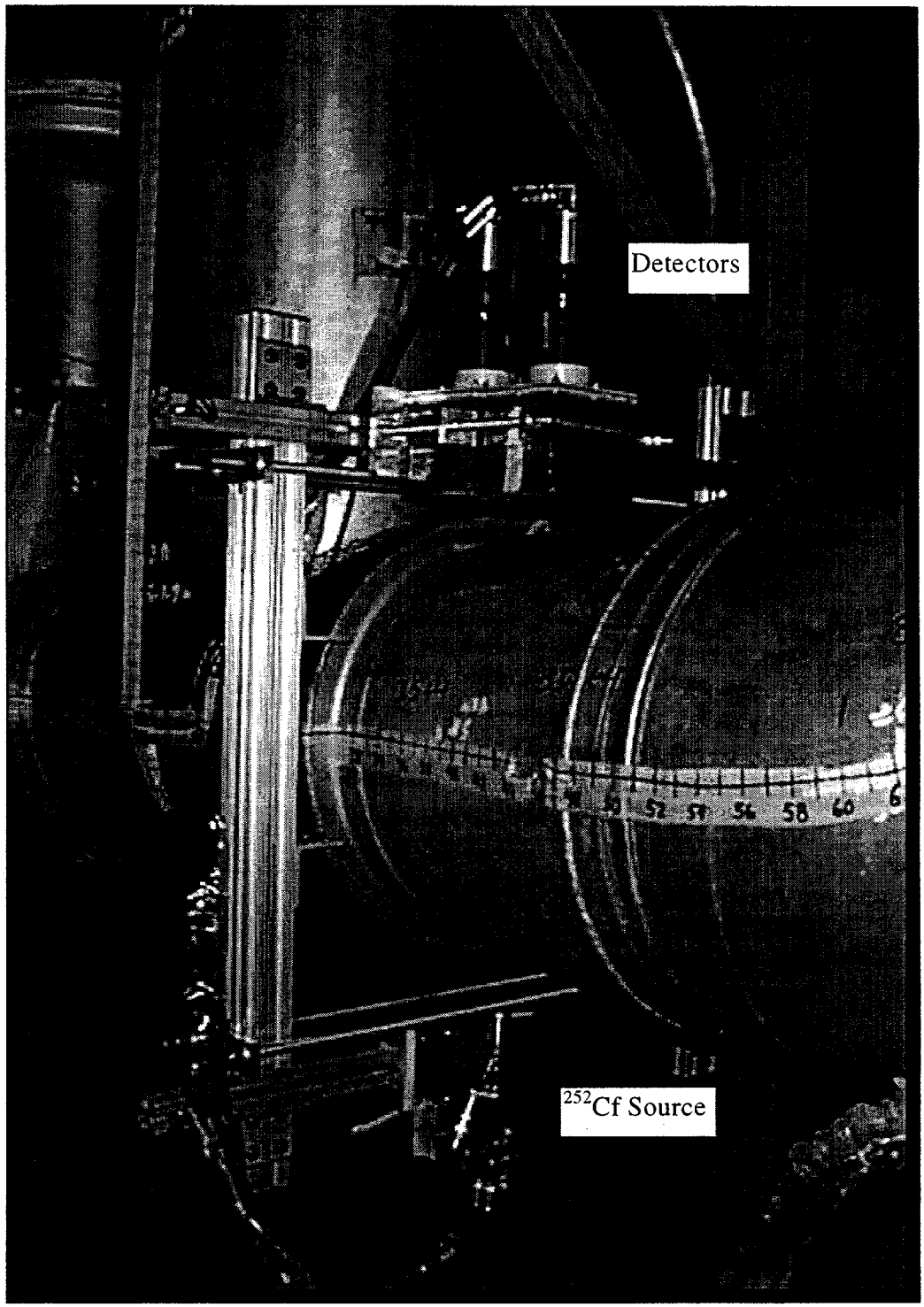

Figure 2

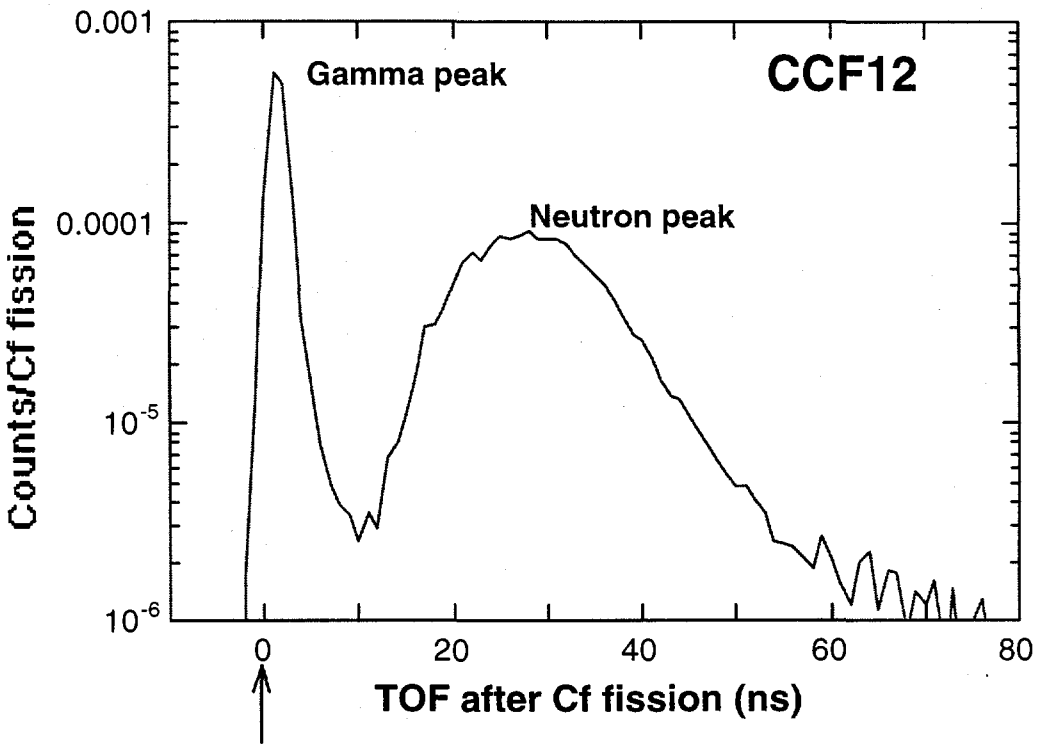
0.001
0.0001
10^{-5}
10^{-6}
Counts/Cf fission
Gamma peak
CCF12
Neutron peak
0
20
40
60
80
TOF after Cf fission (ns)

Figure 3

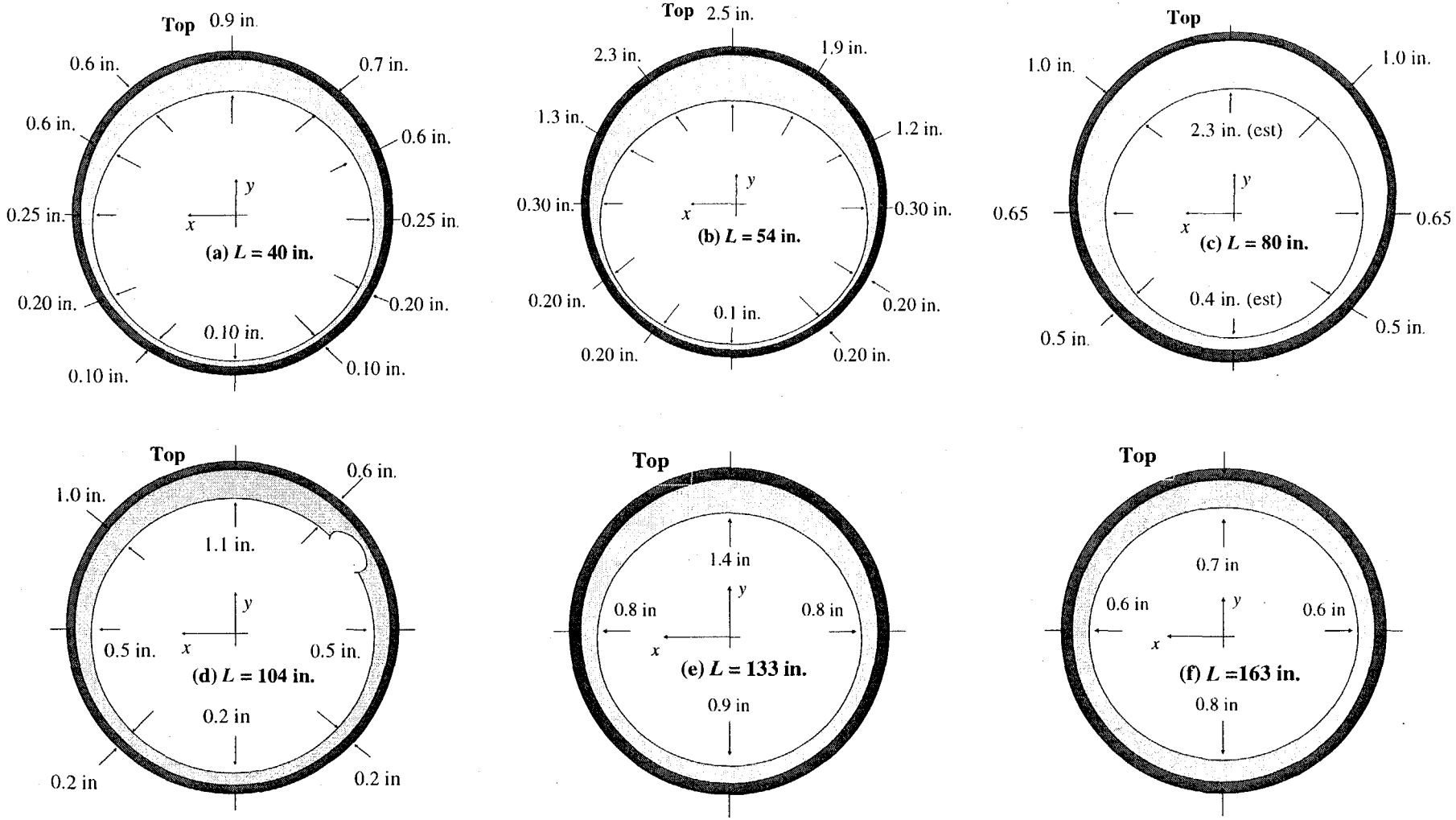
Top
0.9 in.
0.6 in.
0.7 in.
0.6 in.
0.6 in.
0.25 in.
0.25 in.
y
x
(a) L = 40 in.
0.20 in.
0.20 in.
0.10 in.
0.10 in.
0.10 in.
Top
2.5 in.
2.3 in.
1.9 in.
1.3 in.
1.2 in.
0.30 in.
0.30 in.
y
x
(b) L = 54 in.
0.20 in.
0.1 in.
0.20 in.
0.20 in.
0.20 in.
Top
1.0 in.
1.0 in.
2.3 in. (est)
0.65
0.65
y
x
(c) L = 80 in.
0.4 in. (est)
0.5 in.
0.5 in.
Top
0.6 in.
1.0 in.
1.1 in.
y
0.5 in.
x
0.5 in.
(d) L = 104 in.
0.2 in
0.2 in
0.2 in
Top
1.4 in
y
0.8 in
0.8 in
x
(e) L = 133 in.
0.9 in
Top
0.7 in
0.6 in
y
0.6 in
x
(f) L =163 in.
0.8 in

Figure 4

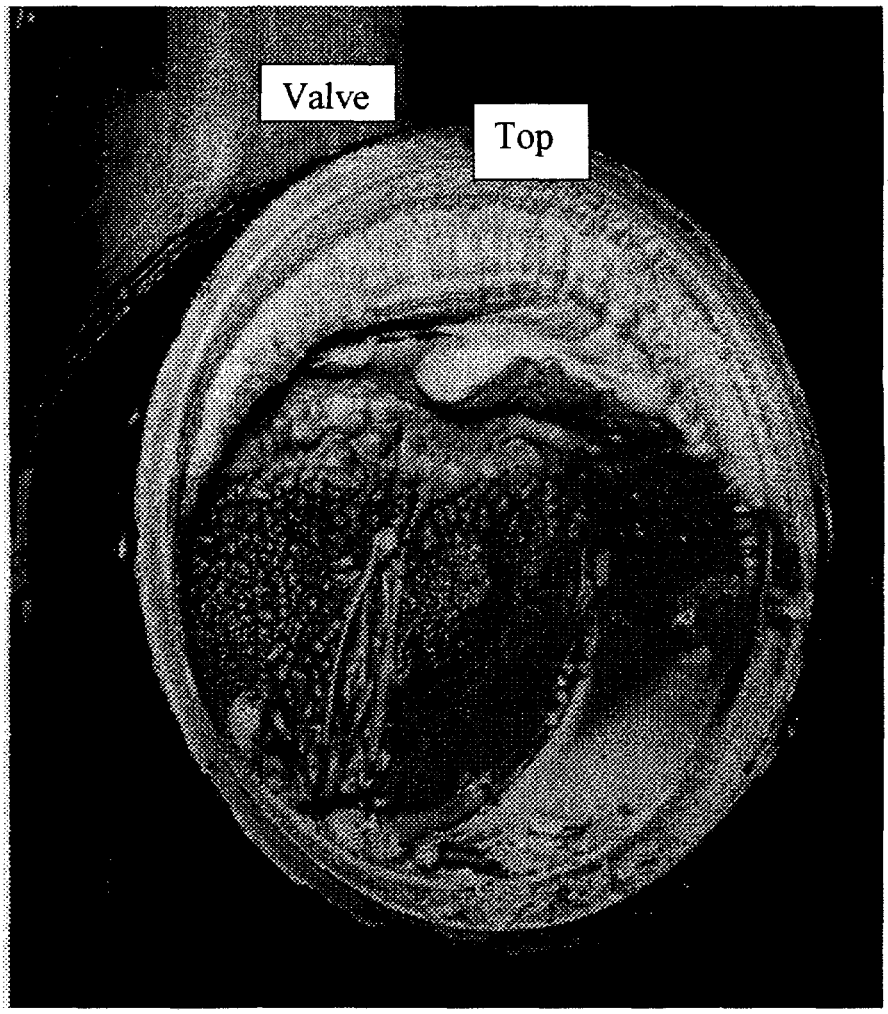

Figure 5

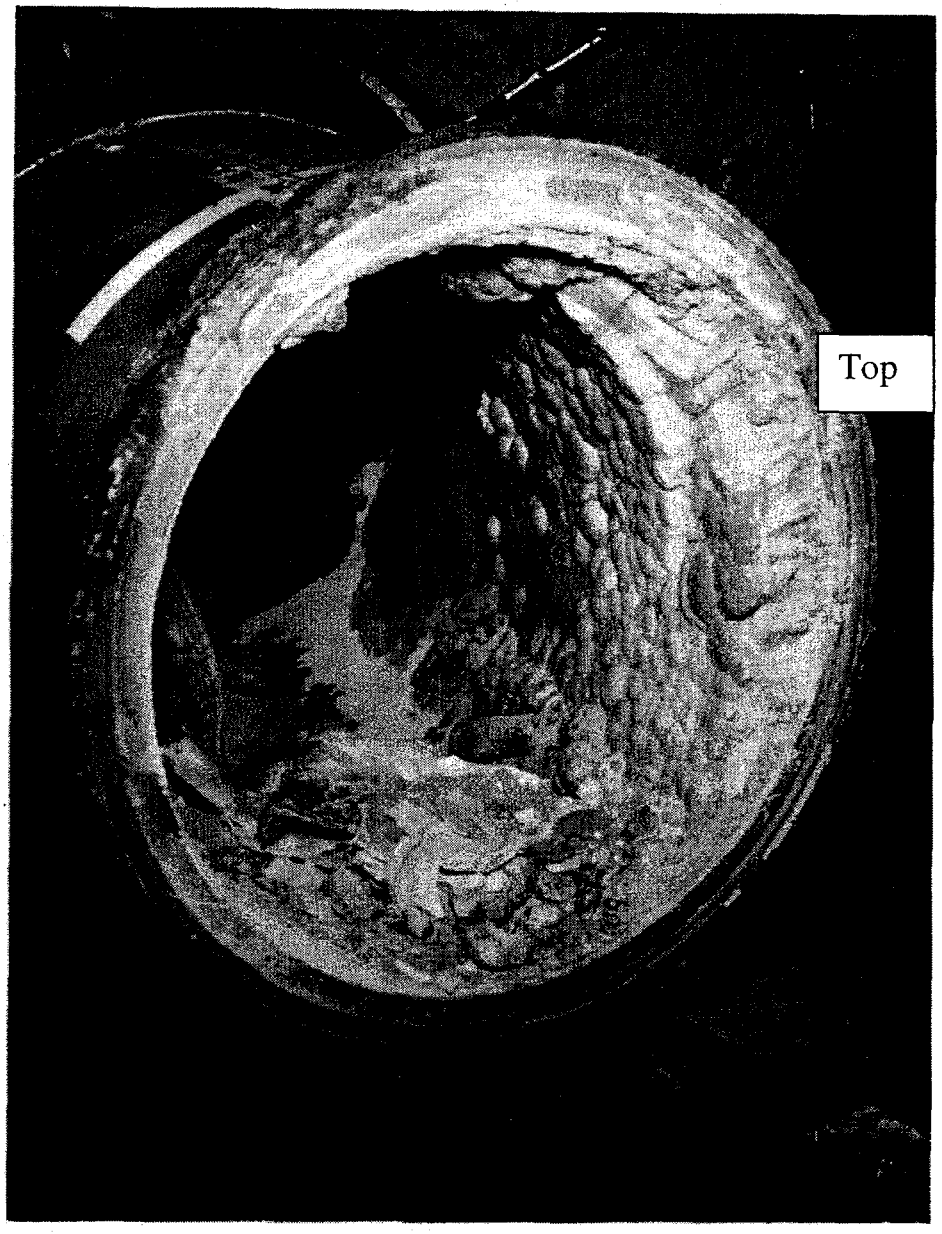

Figure 6

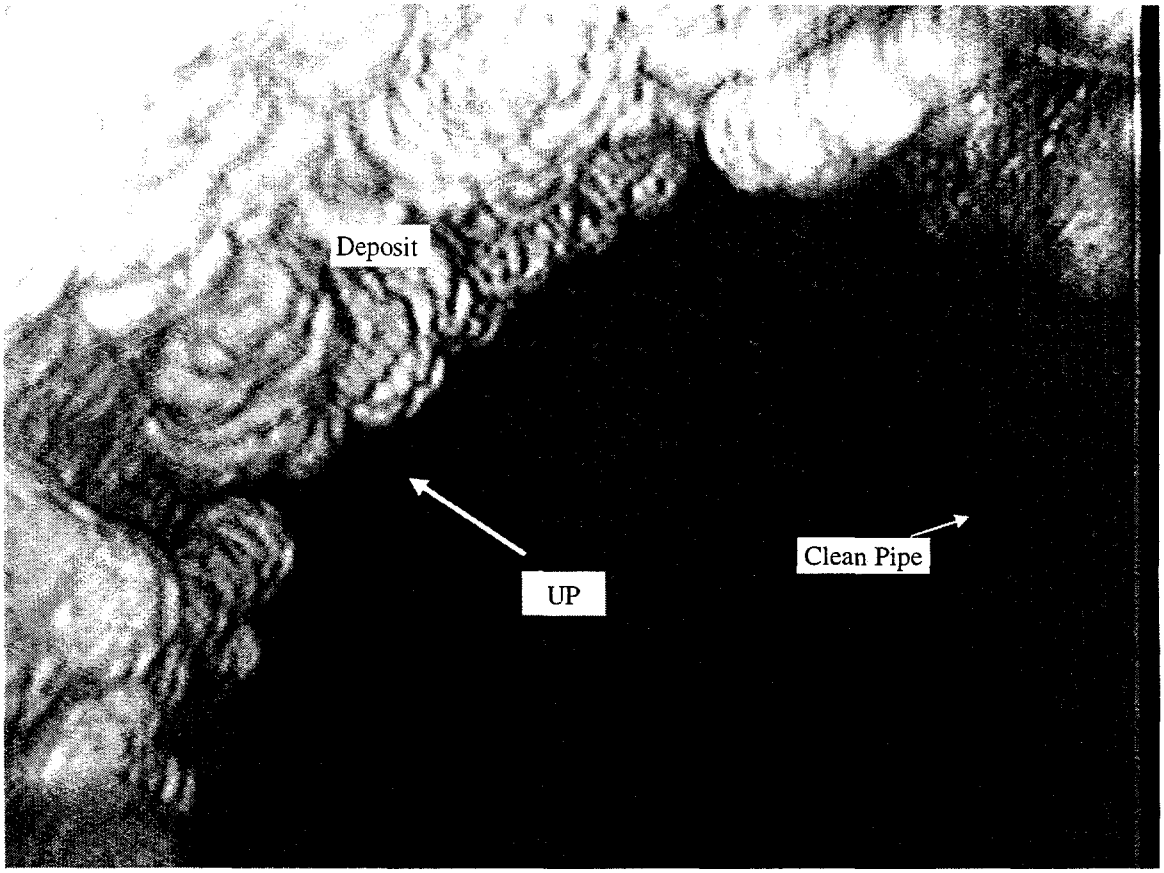

Figure 7

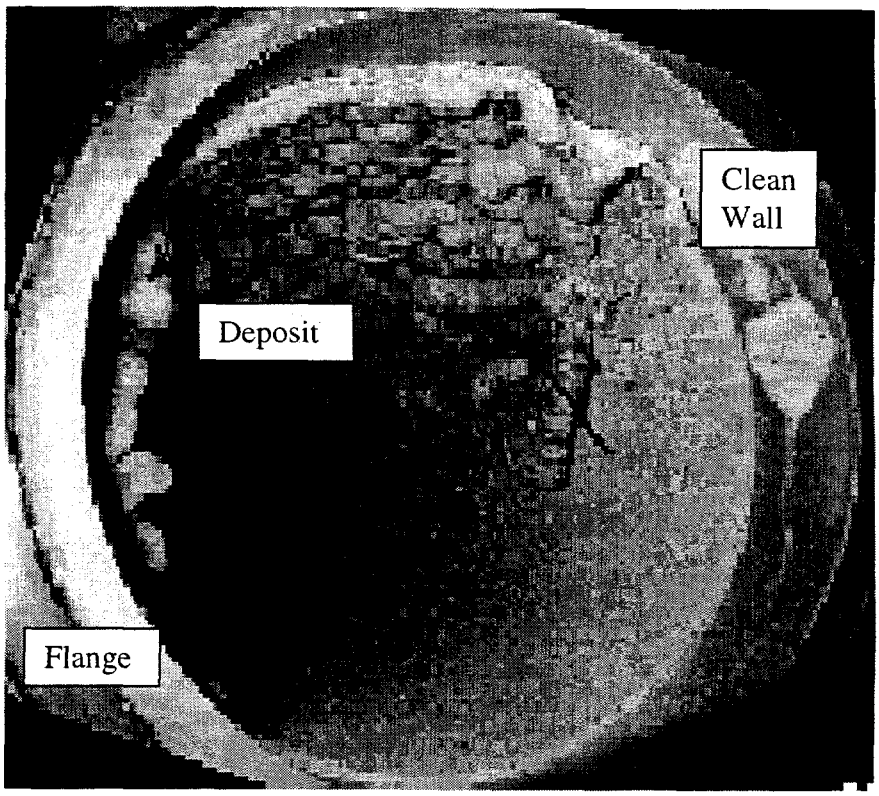

Figure 8